lubricants

MDPI

Article

Investigating Influence of Mo Elements on Friction and Wear Performance of Nickel Alloy Matrix Composites in Air from 25 to 800 °C

Jinming Zhen *, Yunxiang Han, Lin Yuan, Zhengfeng Jia and Ran Zhang

College of Materials Science and Engineering, Liaocheng University, Liaocheng 252059, China; hanyxd@163.com (Y.H.); 19111912571@163.com (L.Y.); jiazhfeng@lcu.edu.cn (Z.J.); zhangranlicp@163.com (R.Z.)
* Correspondence: zhenjinming@lcu.edu.cn; Tel.:+86-13563040259

Abstract: Rapid developments in aerospace and nuclear industries pushed forward the search for high-performance self-lubricating materials with low friction and wear characteristics under severe environment. In this paper, we investigated the influence of the Mo element on the tribological performance of nickel alloy matrix composites from room temperature to 800 °C under atmospheric conditions. The results demonstrated that composites exhibited excellent lubricating (with low friction coefficients of 0.19–0.37) and wear resistance properties (with low wear rates of 2.5–28.1 × 10^{-5} mm^3/Nm), especially at a content of elemental Mo of 8 wt. % and 12 wt. %. The presence of soft metal Ag on the sliding surface as solid lubricant resulted in low friction and wear rate in a temperature range from 25 to 400 °C, while at elevated temperatures (600 and 800 °C), the effective lubricant contributed to the formation of a glazed layer rich in $NiCr_2O_4$, BaF_2/CaF_2, and Ag_2MoO_4. SEM, EDS, and the Raman spectrum indicated that abrasive and fatigue wear were the main wear mechanisms for the studied composites during sliding against the Si_3N_4 ceramic ball. The obtained results provide an insightful suggestion for future designing and fabricating solid lubricant composites with low friction and wear properties.

Keywords: nickel-based alloy; Mo element; high temperature; friction

check for updates

Citation: Zhen, J.; Han, Y.; Yuan, L.; Jia, Z.; Zhang, R. Investigating Influence of Mo Elements on Friction and Wear Performance of Nickel Alloy Matrix Composites in Air from 25 to 800 °C. *Lubricants* **2024**, *12*, 396. https://doi.org/10.3390/lubricants12110396

Received: 17 October 2024
Revised: 10 November 2024
Accepted: 15 November 2024
Published: 18 November 2024

Copyright: © 2024 by the authors. Licensee MDPI, Basel, Switzerland. This article is an open access article distributed under the terms and conditions of the Creative Commons Attribution (CC BY) license (https://creativecommons.org/licenses/by/4.0/).

1. Introduction

High-performance materials with excellent tribological properties have recently become urgently needed due to rapid developments in the aerospace, nuclear, and automobile industries [1–7]. The moving parts of nuclear reactors, petrochemical equipment, steam power plants, aircraft engines, and various types of gas turbines need maintenance under severe conditions (high temperature, corrosive gasses, vacuum, radiation, etc.). Introducing solid lubricants, e.g., metal oxides (MoO_3, NiO, CuO, Fe_2O_3, etc.), noble metals (Au, Ag, Cu, etc.), transition-metal dichalcogenides (WS_2, MoS_2, $MoSe_2$, etc.), and alkaline halides (e.g., BaF_2, CaF_2, CeF_2, etc.), into composites is the most effective way to increase lubricating and wear-resistance properties for composites used in moving parts [8–15]. Traditional lubricating agents, such as oil/grease and polymer matrix composites, carbonize/decompose in harsh environments and lose their lubrication ability, failing to protect moving parts from potential accidents. Therefore, developing high-performance solid lubrication composites is urgently needed.

The two most famous wide-temperature solid lubricants were plasma spray (PS) and adaptive nano-lubricating coatings, which were fabricated by the National Aeronautics and Space Administration and the Air Force Research Laboratory, respectively. The former PS coatings were successfully applied as components of foil bearings and lightly loaded oscillatory bearings. They were developed in four generations, from the PS100 to the PS400 series [16–21]. These coatings exhibited excellent wear resistance and lubricating performance in broad temperatures for the first time by employing $Ag/BaF_2{\cdot}CaF_2$ as solid

lubricants (soft metal Ag as low-to-moderate temperature, and $BaF_2{\cdot}CaF_2$ as a moderate-to-high temperature), glass/Cr_2O_3/Cr_2C_3 as a reinforcing phase, and nickel alloy as a matrix. The latter adaptive nanocomposite tribological coatings, also called "chameleon" coatings, because these coatings could respond to surrounding environments by adjusting the contact surface compositions and microstructure of (like a chameleon changing its skin color to avoid) to maintain good self-lubricating properties under testing conditions (such as humid/dry cycling and temperature variation). Results showed that the adaptive self-lubricating mechanism combined the chemical composition (containing low melting point oxide, bimetallic oxide, and layer structure material) and surface structure (gradient interface, two-layer coating with a patterned diffusion barrier) to the main low friction and wear rate. These coatings include DLC/TiC/WC, YSZ/Ag/Au, YSZ/Ag/Mo/MoS_2, YSZ/Au/MoS_2/DLC, VN/Ag, (Ag, Cu)-Ta-O, etc. [2,9,22–28].

Besides these two best examples, many other solid lubricating composites were also developed [29–32]. To increase the high-temperature wear performance of tool materials, Ripoll et al. fabricated NiCrSiB-Ag-MoS_2 mm-thick coatings using laser metal deposition [12]. The effective lubricant at elevated temperatures (600–800 °C) resulted in a glazed tribolayer rich in silver molybdate. Bian et al. prepared a NiCr-Cr_3C_2 coating in fluoride molten salts using high-speed laser cladding, and the results showed that the composite coating that contained 60 wt. % Cr_3C_2 exhibited quite a low wear rate of 2.78×10^{-6} mm^3/Nm and friction coefficient of 0.12 [33]. Ye et al. studied Ag content on wear resistance of Ni60 coatings at different temperatures, finding that the oxide lubrication layer formation rich in Ag_2O, NiO, and $AgCrO_2$ was beneficial for high temperature tribological behavior [34]. Using the spark plasma sintering method, Zeng et al. prepared a nickel-based h-BN/$CePO_4$ composite coating, and the high-temperature friction and wear results indicated that the formation of gradient lubrication film formed on the sliding surface exhibited the best lubricating properties [35]. Employing a laser cladding method, Zheng et al. fabricated Ni60/WC-Cu/MoS_2 composite coatings. Cu and MoS_2 decreased the wear rate for the coating due to the formation of the uniformly distributed self-lubricating film rich in MoS_2 and the structural enhancement by Cu, which induced solid solution strengthening and minimized wear debris generation [36].

In addition, due to dispersion strengthening and alloying, it is important to investigate how the amount of a specific element influences the tribological performance of composites. Qin et al. studied Mo content on the wear resistance of iron matrix materials, and the results demonstrated that due to the strengthening effects of Mo, composites that contain 12% Mo had the lowest wear rate [37]. Using the high-velocity oxy-fuel process, Behera et al. prepared two composite coatings (WC-CoCr/Mo and WC-Co/NiCr/Mo), and studied the Mo addition on the wear behavior for the coatings. The results showed that the WC-CoCr coating with 10% Mo had the best frictional performance at high temperatures, and this was mainly due to the thin oxide layer which formed on the contact surface rich in WO_3, $CoWO_4$, MoO_3, $NiMoO_4$, and $CoMoO_4$ [38]. Zhu et al. prepared high-entropy carbide materials and investigated the Ag and Mo content on its frictional behavior [29], and the results demonstrated that the formed multi-component lubricating film significantly improved the wide-temperature wear resistance, especially at 300 °C. To improve the poor friction behavior of titanium alloys, Zhen et al. fabricated a multiphase Ti-Mo-Ag composite via the spark plasma sintering method, and the results showed that a heterogeneous triple-phase co-reinforced microstructure was formed, which demonstrated the Ti-Mo-Ag composite lubricating performance at 600 °C (friction coefficient: 0.20, wear rate: 8.0×10^{-6} mm^3/Nm) [39]. Moussaoui et al. studied the effect of the addition of Mo on the mechanical and frictional behavior of TiN film, and the results indicated that the mechanical/wear resistance performance was significantly enhanced as the Mo content is 18 at.% due to the solid solution of nitride mixture phase of TiN/MoN [40]. Cui et al. designed and prepared a Stellite 12 alloy/Mo coating by laser cladding; the friction and wear properties from 25 to 1000 °C were significantly enhanced due to the complex carbides (with net structure and high hardness/load-carrying) and the formation of a lubricating

film. The coating with 12.0 wt. % Mo exhibited optimal wide-temperature tribological performance [41].

In a previously reported study, the influence of Mo on the high-temperature frictional performance for NiCrMoTiAl matrix composites was investigated in vacuum. To systematically investigate the tribological properties of these composites, high-temperature wear behavior was investigated from 25 to 800 °C under atmospheric conditions in this study, and the obtained data were compared. Furthermore, the influence of contact surface oxidation on the wear and lubricant mechanism was also discussed in detail.

2. Experimental Details

2.1. Materials

Using a hot-pressing sintering method, the nickel alloy matrix composite was fabricated by mixing nickel alloy powder and solid lubricant (Ag and BaF_2/CaF_2). The detailed processing parameters were described elsewhere [42]. Table 1 lists the composition of the prepared composite samples.

Table 1. Compositions of the composites [42].

Composites	Ni Alloy	BaF_2/CaF_2 (wt. %)	Ag (wt. %)	Density (g/cm^3)
0Mo	Ni15Cr3Ti6Al	5	12.5	7.46
5Mo	Ni15Cr5Mo3Ti6Al	5	12.5	7.46
8Mo	Ni15Cr8Mo3Ti6Al	5	12.5	7.37
12Mo	Ni15Cr12Mo3Ti6Al	5	12.5	8.04

2.2. Tribological Tests

Tribological tests were performed on an HT-1000 ball-on-disk (Lanzhou Zhongke Kaihua Technology Development Co., Ltd., Lanzhou, China) high-temperature tribometer. All composite disks were polished carefully using abrasive paper and metallographic abrasive paper, and the Si_3N_4 ball (6.35 mm, 1500HV1) was used as the counterpart material for its aerospace applications. The tribotests were run in the air under the following conditions: sliding speed of1.0 m/s, duration of 30 min, normal load of 5 N, and 10 mm wear track diameter. The testing temperatures were selected as 25, 200, 400, 600 and 800 °C with a heating rate of 10 °C/min. The friction coefficient (COF) was automatically continuously recorded by computer during the sliding process. The volume of the wear track was measured by a contact surface profilometer, and the value was calculated automatically and expressed in $mm^3N^{-1}m^{-1}$. To ensure the accuracy of the tribological tests, the measurements were performed at least three times under the same conditions.

2.3. Characterization

To further analyze the wear and lubricating mechanism of the nickel alloy matrix composites, the microstructure, worn surface characteristics, and the chemical evolution of the worn surface were investigated by scanning electron microscopy (SEM, JSM 5600LV, Zeiss, Jena, Germany) with energy-dispersive spectrometry (EDS) and LabRAM HR evolution Micro-Raman spectrometry (Renishaw inVia Reflex, with a wavelength of 532 nm, Wotton-under-Edge, UK).

3. Results and Discussion

Figure 1 shows the evolution of COF vs. testing temperature for the four composites under atmospheric conditions. All four composites show excellent lubricating properties from 25 to 800 °C, and the value fluctuates between 0.19 and 0.37. The COF values change similarly with temperature for all investigated composites: from 25 to 200 °C, the COFs of the composites decrease to minimum values (0Mo: 0.36–0.2; 5Mo: 0.36–0.22; 8Mo: 0.37–0.27; 12Mo: 0.27–0.19); when the testing temperature increases to 600 °C, the COF values continuously increase (0Mo: 0.29; 5Mo: 0.28; 8Mo: 0.33; 12Mo: 0.25), then

they decrease somewhat at 800 °C (0Mo: 0.24; 5Mo: 0.23; 8Mo: 0.29; 12Mo: 0.23). This phenomenon may be explained as follows: from 25 to 200 °C, the soft metal Ag diffusion rate from the matrix to the sliding surface increases, thus resulting in decreased COFs; when the test temperature is 400 and 600 °C, the oxidation of the contact surface limits the diffusion of solid lubricants to some extent, so the COFs increase; at 800 °C, the formation of a continuous glaze layer decreases the COF values (which will be showed in the SEM image below). By comparison, 12Mo composite exhibits the lowest COF, while 8Mo has the highest COF and 0Mo/5Mo composites exhibited similar COFs under the given test conditions.

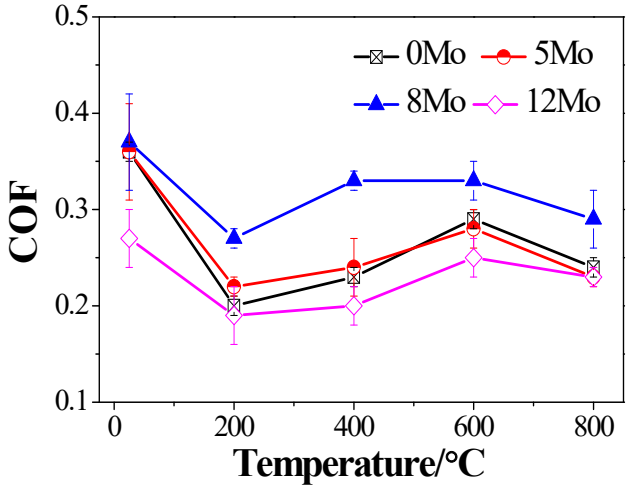

Figure 1. COF vs. testing temperature of nickel alloy matrix composites.

Moreover, when compared with the values under vacuum condition [32], we can see that all four composites exhibit relatively high COFs from 25 to 600 °C, especially at 600 °C, as the value is below 0.2 in vacuum. As the surrounding temperature increases to 800 °C, the trend is the opposite; all four composites exhibit higher COF values in a vacuum than that in the air. This may be explained by an increased diffusion rate of solid lubricants from the matrix toward the contact surface as testing temperature increases from 25 to 600 °C, keeping in mind that oxidation is limited under vacuum conditions, so the COFs are low. At 800 °C, significantly decreased hardness, and mechanical properties in general, result in the highest COF values.

The wear rate vs. testing temperature curves for the four composites coupled with a Si_3N_4 counterpart material are shown in Figure 2. All four composites present low wear rates under atmospheric conditions, the value is in the order of 10^{-5} mm^3/Nm (2.5–28.1 $\times$ 10^{-5} mm^3/Nm), especially for 8Mo and 12Mo composites, being below 8.8 $\times$ 10^{-5} mm^3/Nm. Regarding the temperature effect, from 25 to 200 °C, the wear rate decreases first for 0Mo and 5Mo composites; then it increases continuously and reaches a maximum at 600 °C (0Mo: 18.4 $\times$ 10^{-5} mm^3/Nm, 5Mo: 28.1 $\times$ 10^{-5} mm^3/Nm); as the testing temperature increases to 800 °C, the wear rate decreases to a certain extent. As for 8Mo and 12Mo composites, the values increase gradually to the maximum as temperature increases to 400 °C (8Mo: 8.8 $\times$ 10^{-5} mm^3/Nm) and 600 °C (12Mo: 8.4 $\times$ 10^{-5} mm^3/Nm); at 800 °C, due to the glazed layer forming on the sliding surface, these two composites exhibit high wear resistance properties. Regarding the effect of the Mo content from 25 to 600 °C, 8Mo and 12Mo composites exhibit a relatively low wear rate, while at 800 °C, the 0Mo composite shows the best wear resistance properties. Also, all composites have higher wear rates from 25 to 600 °C under air than that under vacuum conditions.

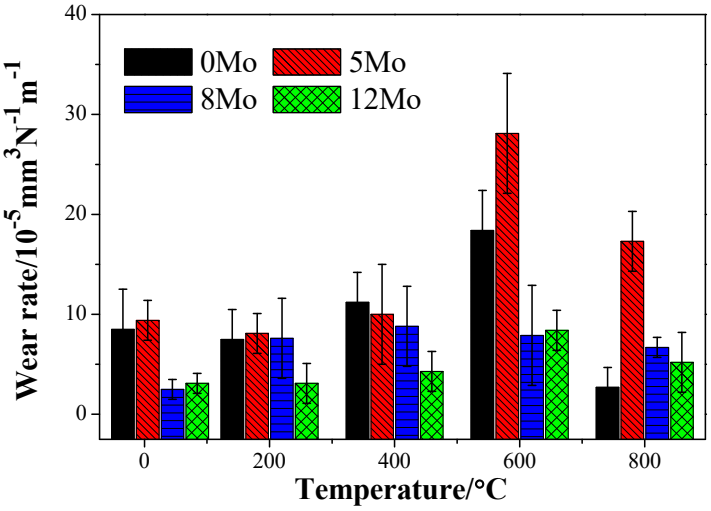

Figure 2. COF vs. testing temperature of nickel alloy matrix composites.

The wear resistance properties for the investigated composites can also be reflected in three-dimensional morphologies, as shown in Figures 3 and 4. At 25 °C, the wear track is covered with wide/shallow grooves for 0Mo (Figure 3a) and narrow/deep grooves for 5Mo (Figure 3e). For 8Mo and 12Mo composites (Figure 4a,e), the groove depth is about 20 μm, which is quite lower than that of 0Mo and 5Mo. As the testing temperature increases to 400/600 °C, the wear track becomes larger and deeper for all four composites as compared to that at 25 °C (Figure 3b,c,e,f and Figure 4b,c,e,f), which can be attributed to matrix softening. At 800 °C, the worn track is shallow at 800 °C for all composites due to the formation of the oxidative glazed layer.

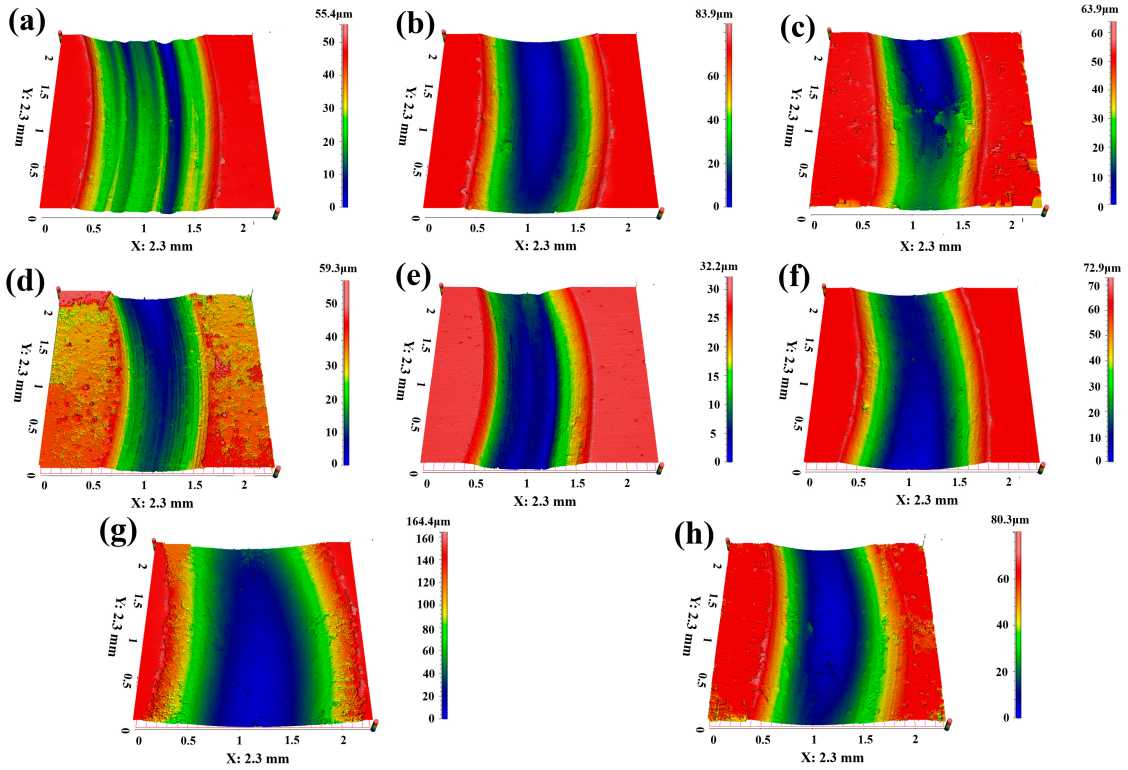

Figure 3. Three-dimensional morphologies of worn surface for 0Mo and 5Mo composites: (**a**) 0Mo 25 °C, (**b**) 0Mo 400 °C, (**c**) 0Mo 600 °C, (**d**) 0Mo 800 °C; (**e**) 5Mo 25 °C, (**f**) 5Mo 400 °C, (**g**) 5Mo 600 °C, (**h**) 5Mo 800 °C.

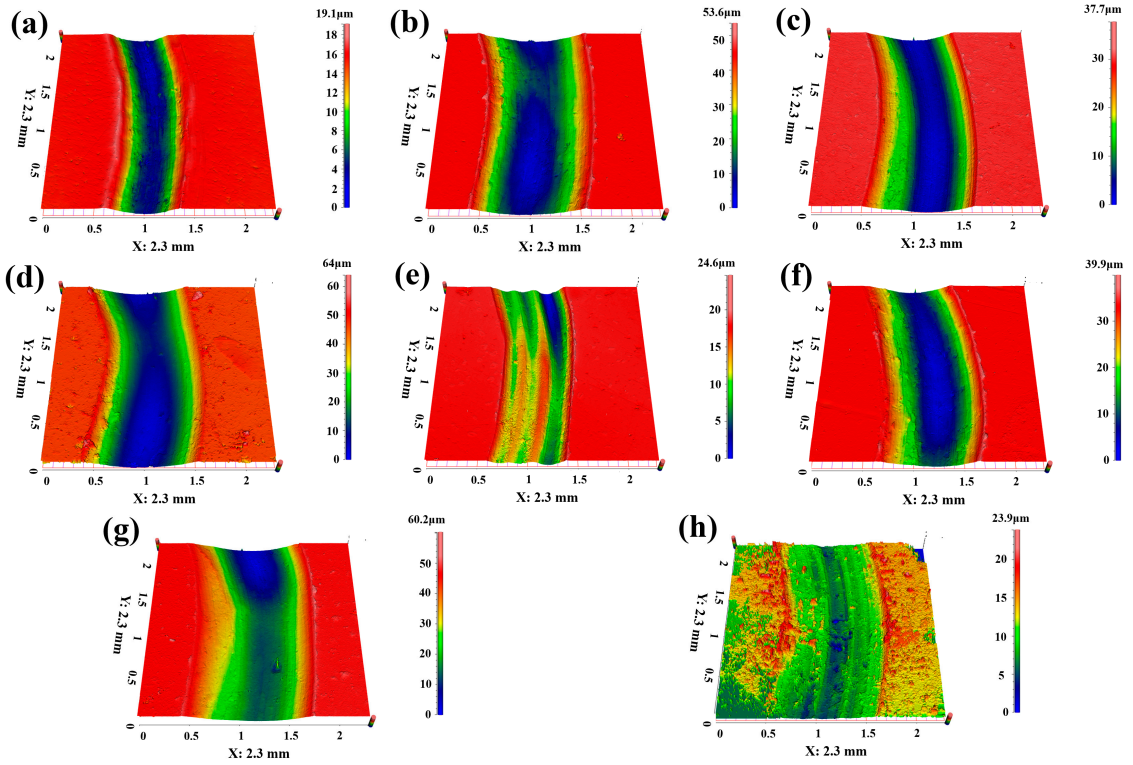

Figure 4. Three-dimensional morphologies of worn surface for 8Mo and 12Mo composites: (**a**) 8Mo 25 °C, (**b**) 8Mo 400 °C, (**c**) 8Mo 600 °C, (**d**) 8Mo 800 °C; (**e**) 12Mo 25 °C, (**f**) 12Mo 400 °C, (**g**) 12Mo 600 °C, (**h**) 12Mo 800 °C.

For the analysis of the wear mechanism at various temperatures from 25 °C to 800 °C for the composites, SEM images were investigated, as shown in Figures 5–8. For the 0Mo composite, grooves and wear debris appeared on the sliding surface (Figure 5a); as the Mo content increases to 5 and 12 wt. % (Figure 5b,c), grooves become the main feature. Overall, the characteristics of the worn surface indicate that abrasive wear is the main wear mechanism for 0Mo and abrasive/fatigue wear for 5Mo and 8Mo composites at 25 °C.

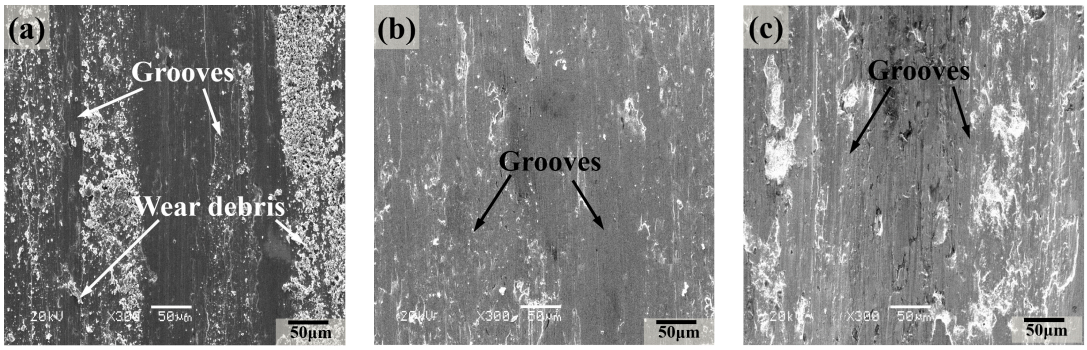

Figure 5. SEM images of worn surfaces for composites at 25 °C: (**a**) 0Mo, (**b**) 5Mo, (**c**) 12Mo.

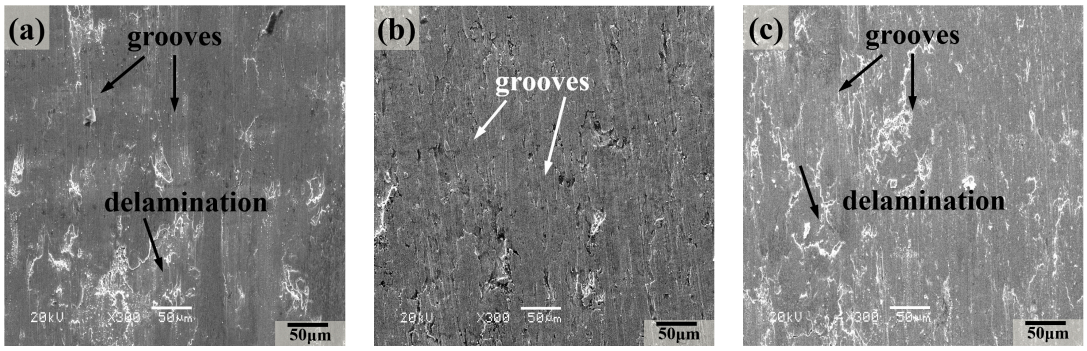

Figure 6. SEM images of worn surfaces for composites at 400 °C: (**a**) 0Mo, (**b**) 5Mo, (**c**) 8Mo.

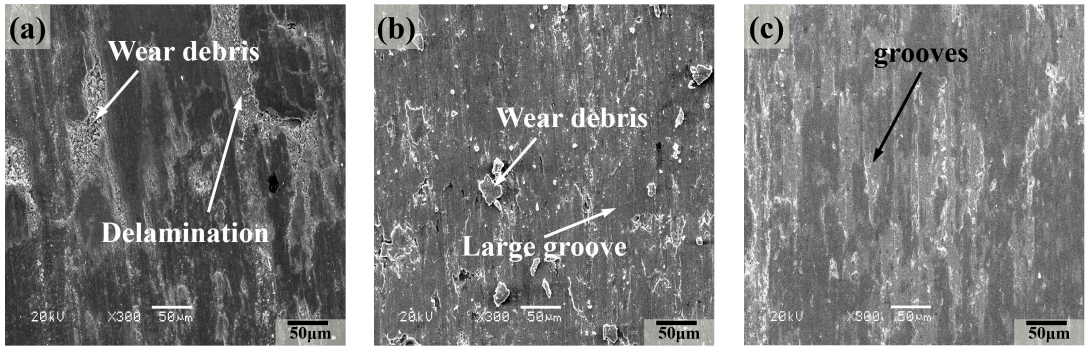

Figure 7. SEM images of the worn surfaces for the composites at 600 °C: (**a**) 0Mo, (**b**) 5Mo, (**c**) 8Mo.

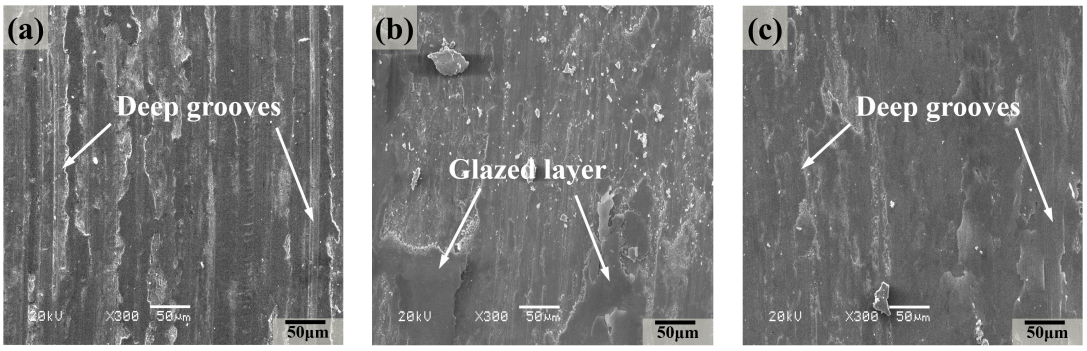

Figure 8. SEM images of the worn surfaces for the composites at 800 °C: (**a**) 0Mo, (**b**) 5Mo, (**c**) 8Mo.

0Mo and 5Mo composites exhibit different worn surface morphologies at 400 °C. As compared with that at 25 °C, delamination appears on the worn surface apart from tiny grooves for 0Mo composite, which suggests that abrasive and fatigue wear are the main wear mechanism (Figure 6a). For 5Mo and 8Mo composites, large grooves indicate that the main wear mechanism is abrasive wear (Figure 6b,c).

Figures 7 and 8 show the worn surfaces of 0Mo, 5Mo, and 8Mo composites coupled with a Si_3N_4 ceramic ball at 600 and 800 °C. Deformation and some wear debris smear on the worn surface for 0Mo composite (Figure 7a) indicates that the main wear mechanism is fatigue wear. For 5Mo and 8Mo composites, (Figure 7b,c), large grooves with some small pits appear on the worn surface. At 800 °C (Figure 8a), different characteristics are exhibited on the sliding surface: a smooth glazed layer with furrows appears on the contact surface, and there is almost no wear debris smeared on it, especially for 8Mo materials, which indicates that the main wear mechanism is abrasive wear.

Combined with the wear rate trend, this may explain the change in the worn surface from the following aspects: from 25 to 400/600 °C, the hardness and mechanical strength of the composites decrease, and large parts of the oxide layer which formed during the sliding

process on the worn surface are removed, thus large wear rate and grooves/delamination occur at this temperature range. Moreover, as the testing condition increases up to an elevated temperature of 600 °C/800 °C, the contact surface between the sample and ceramic ball is covered with an oxide-glazed lubricating layer and only a small amount of these films is consumed in the process of testing, so excellent lubricating and wear resistance performance is exhibited.

The worn scar for the Si_3N_4 ceramic ball sliding against different composites under various testing temperatures was further investigated by SEM and EDS mapping to analyze the wear behavior, as presented in Figures 9–16. Figures 9–11 show the SEM images of the Si_3N_4 ceramic ball's wear scar as sliding against 0Mo and 5Mo composites under various testing temperatures at 25, 400, and 800 °C and the corresponding EDS mapping at 800 °C. It can be seen that the size of the wear scar for 0Mo and 5Mo composites is similar at 25 and 400 °C, with both exhibiting a large transfer film on the contact surface. As the testing condition increases to 800 °C, the wear scar of 0Mo (Figure 9c) is smaller than that of 5Mo (Figure 9f) and the transfer film is also small; the EDS results indicate that this transfer film is rich in Ni, O, Cr, and Ag elements (Figures 10 and 11). We speculate that the oxide-glazed film formed on the contact surface could increase the wear resistance properties for materials, which is consistent with the wear rate changing trend (Figure 2) [6].

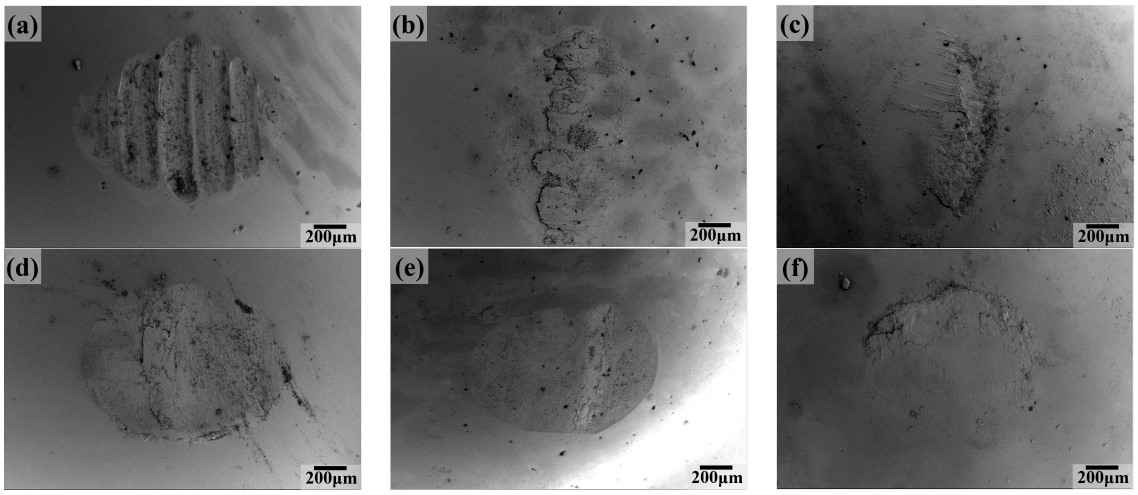

Figure 9. SEM images of worn scar for Si_3N_4 ceramic ball: (**a**) 0Mo 25 °C, (**b**) 0Mo 400 °C, (**c**) 0Mo 800 °C, (**d**) 5Mo 25 °C, (**e**) 5Mo 400 °C, (**f**) 5Mo 800 °C.

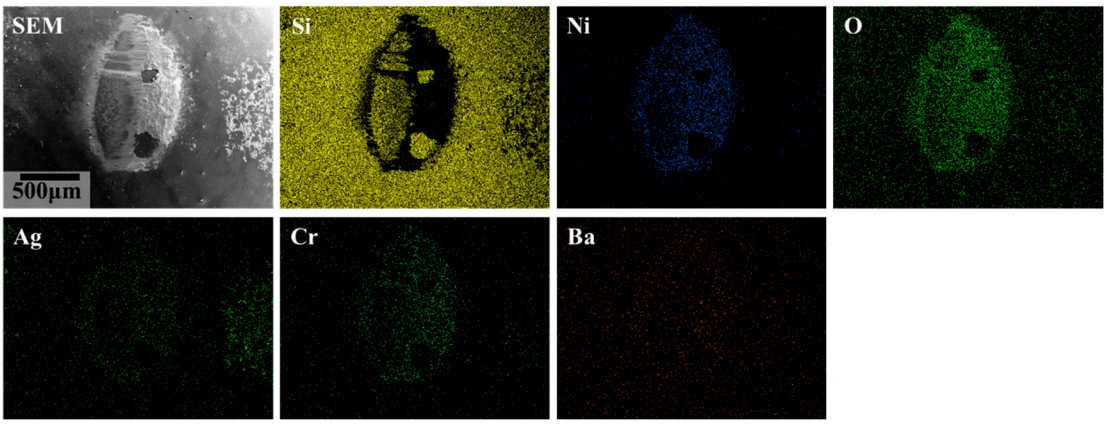

Figure 10. SEM images and corresponding EDS mapping of worn surface for Si_3N_4 ceramic ball sliding against 0Mo composite at 800 °C.

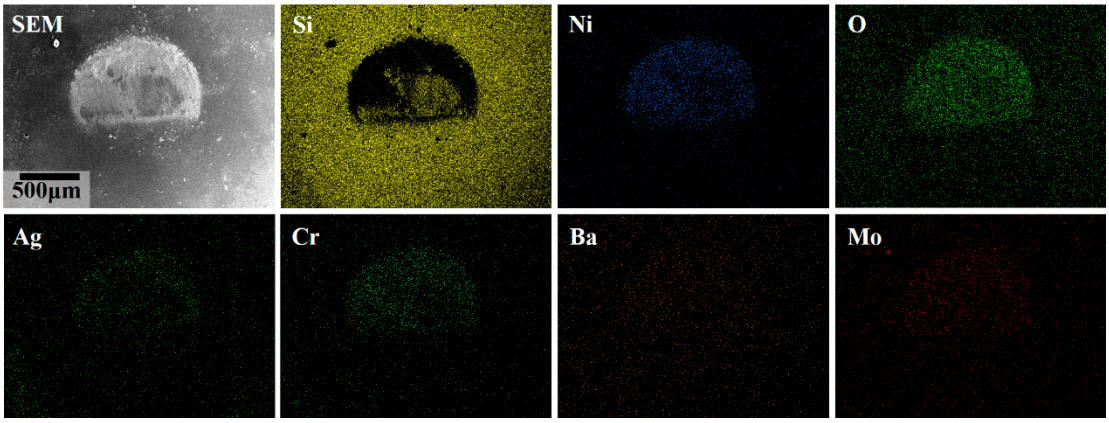

Figure 11. SEM images and corresponding EDS mapping of worn surface for Si_3N_4 ceramic ball sliding against 5Mo composite at 800 °C.

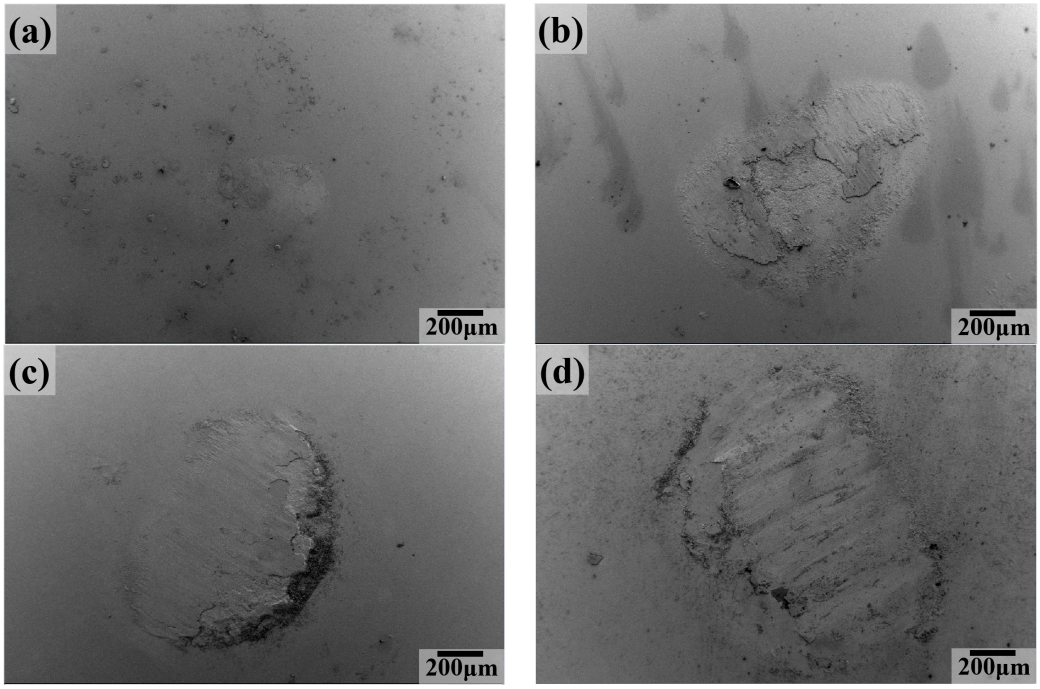

Figure 12. SEM images of worn scar for Si_3N_4 ceramic ball: (**a**) 8Mo 25 °C, (**b**) 8Mo 400 °C, (**c**) 8Mo 800 °C, (**d**) 12Mo 800 °C.

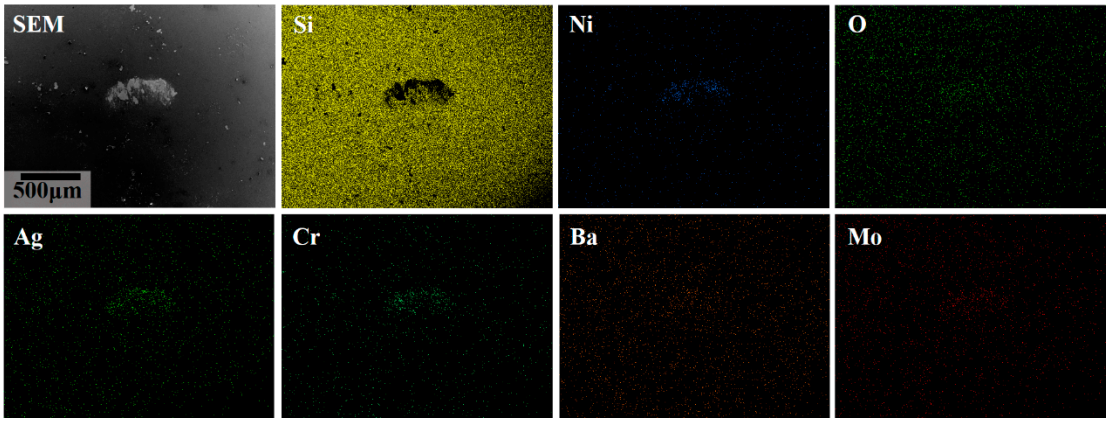

Figure 13. SEM images and corresponding EDS mapping of worn scar for Si_3N_4 ceramic ball sliding against 8Mo composite at 25 °C.

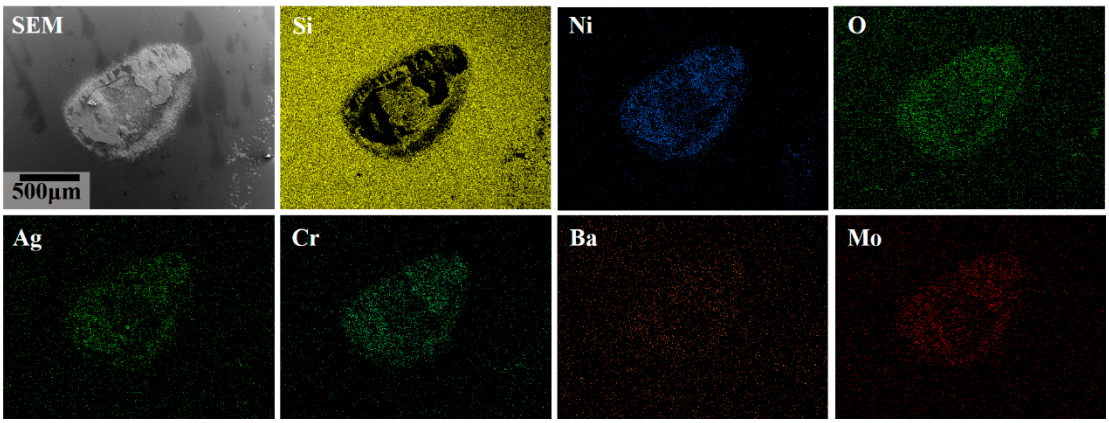

Figure 14. SEM images of worn scar for Si_3N_4 ceramic ball and corresponding EDS mapping coupled with 8Mo composite at 400 °C.

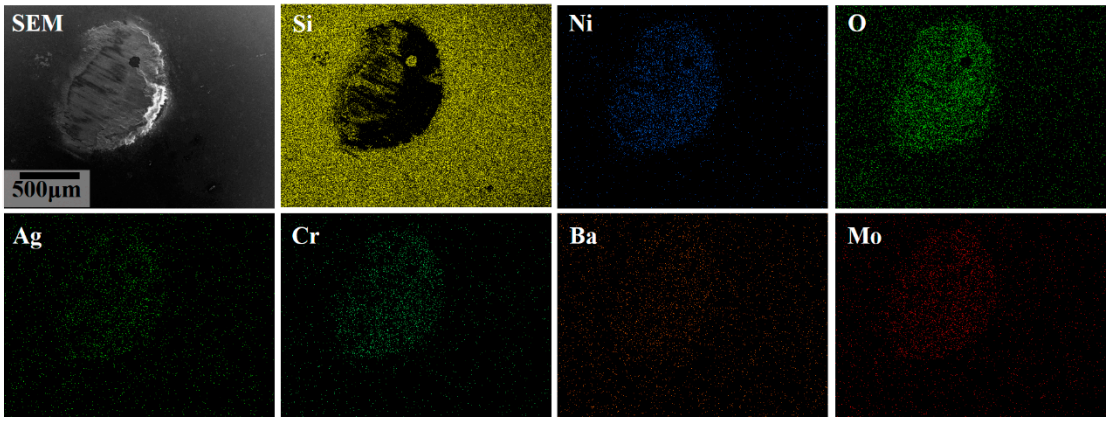

Figure 15. SEM images and corresponding EDS mapping of worn surface for Si_3N_4 ceramic ball coupled with 8Mo composite at 800 °C.

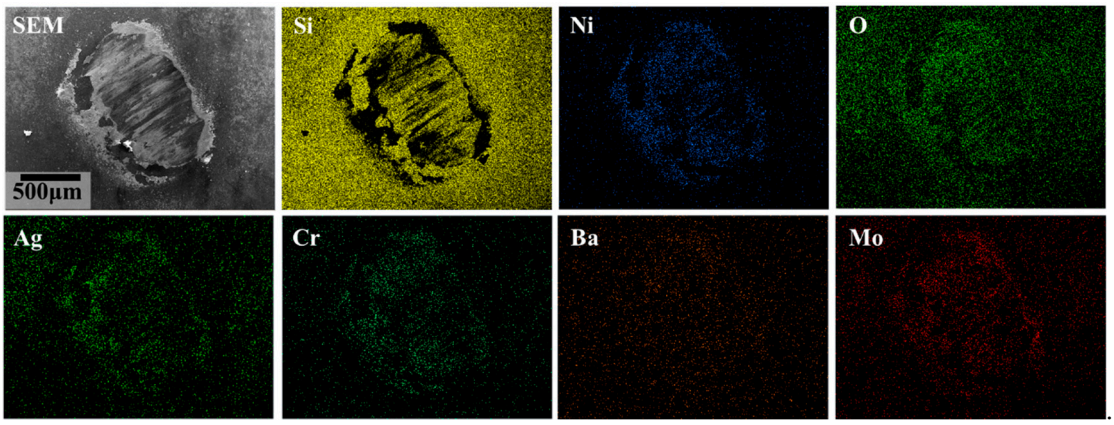

Figure 16. SEM images and corresponding EDS mapping of worn surface for Si_3N_4 ceramic ball sliding against 12Mo composite at 800 °C.

Figures 12–16 show the SEM images of the contact surface of the Si_3N_4 ceramic ball and corresponding EDS mapping sliding against 8Mo and 12Mo composites at 25, 400, and 800 °C. The size of the wear scar at 25 °C (Figure 12a) is small and there is only a small amount of transfer film smeared on the contact surface; this is in agreement with the wear rate changing trend for 8Mo composite. Moreover, EDS mapping results (Figure 13) present that the main elements of the transfer film are Ni, Cr, and Ag, indicating that the

lubricating film is formed on the contact surface, and this may be attributed to the self-lubricating and wear resistance properties at 25 °C. As testing temperature increases to 400, 600, and 800 °C, the size of the worn surface becomes bigger than that at room temperature (Figure 12b–d), and a large transfer film is formed on the Si_3N_4 ceramic ball's contact surface, indicating that metal-to-metal contact occurs during the frictional process, so the relatively high COF and wear rate are exhibited. In addition, the elemental distribution of the contact surface for the Si_3N_4 ceramic ball indicates the presence of Ni, Cr Mo, O, and Ag in the formed tribolayer (Figures 14–16), which suggests that a tribolayer rich in these compositions is formed and this is attributes to the friction and wear behavior for 8Mo and 12 Mo composites. The Raman spectrum, the SEM images of the worn surface, and the corresponding EDS mapping for four composites at different temperatures were conducted to discuss the wear mechanism, as presented in Figures 17–19. Composites 8Mo and 12Mo showed a smooth glazed layer with a large area of gray glass pattern spot inlaid on the surface. The EDS results show that the main elements of the smooth dark gray area are Ni and O, while the main composition for the light gray spots are Mo, Ba, Ca, and Ti. This indicates that nickel oxide and calcium/barium molybdate are formed on the sliding surface. Figure 19 confirms that the main compositions of the respective worn surfaces at 800 °C for the four composites are $NiCr_2O_4$, Ag_2MoO_4, and $BaMoO_4$ (Figure 19a). It was previously reported that a tribolayer rich in these compounds could effectively lubricate at elevated temperatures, so excellent lubricating and wear resistance performance are exhibited at 800 °C. For 12Mo composite, it can be seen that the oxidation degree increases from 25 to 600 °C, while in this temperature range, during the sliding process, most parts of the oxide layer formed on the contact surface is removed, which is attributed to the contact of ceramic-to-metal and the occurrence of severe deformation/grooves (Figures 5–7).

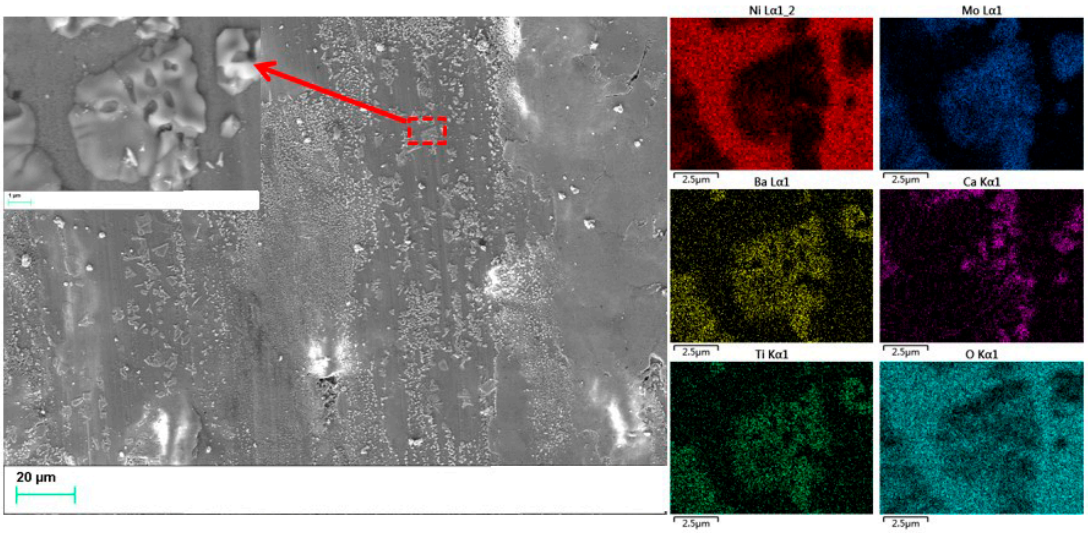

Figure 17. SEM images of 8Mo composite and corresponding element distribution at 800 °C.

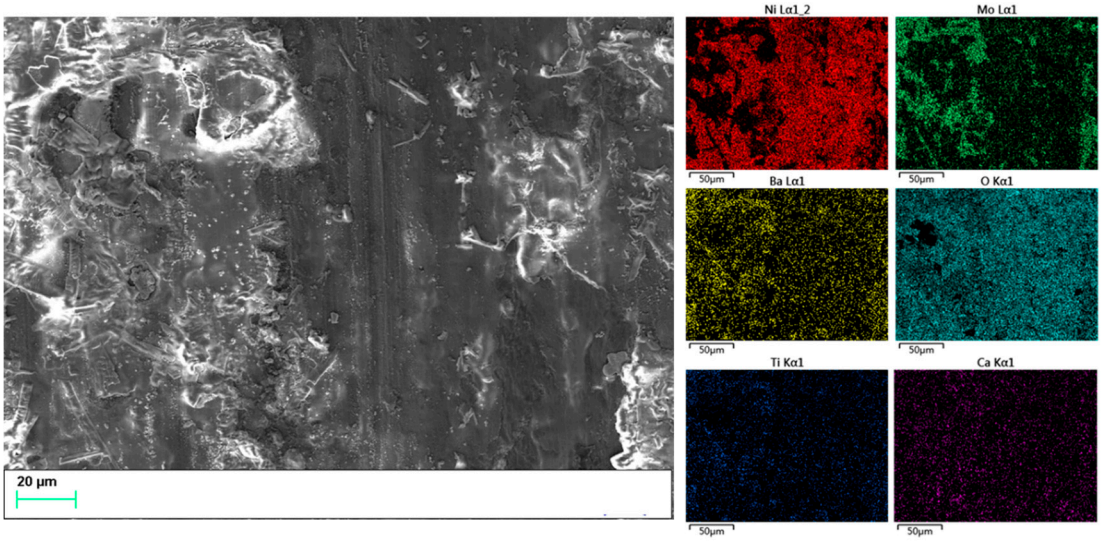

Figure 18. SEM images of sliding surface for 12Mo composite and corresponding element distribution at 800 °C.

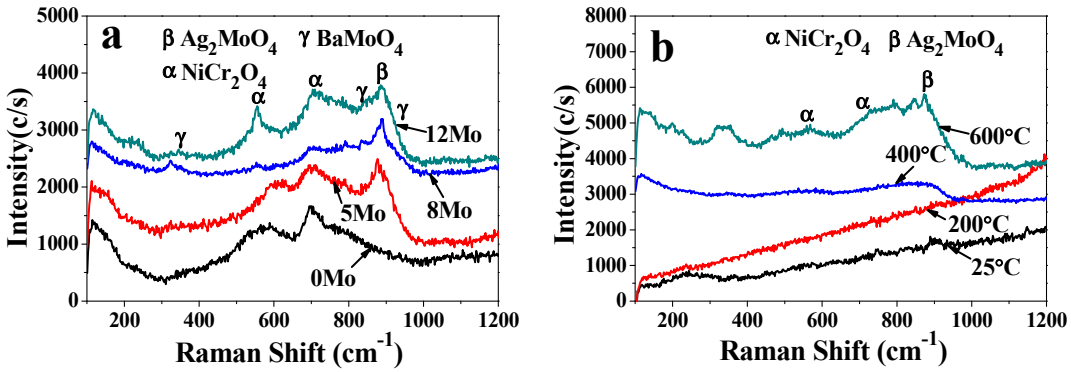

Figure 19. Raman spectrum for nickel alloy matrix composite: (**a**) worn surface for four composites at 800 °C, (**b**) 12Mo composite at 25, 200, 400, and 600 °C.

4. Conclusions

In this study, the NiCrMoTiAl matrix composites with Ag and CaF_2/BaF_2 solid lubricants were prepared, and the effect of the Mo element on tribological performance was studied from 25 to 800 °C under atmospheric conditions. The main conclusions are as follows:

(1) From 25 to 200 °C, the COFs of the studied composites first decreased to the minimum values, and then continuously increased when the temperature increased to 600 °C; at 800 °C, the COF values decreased to a certain extent. Overall, the 12Mo composite showed the lowest COF, while the 8Mo composite exhibited the highest COF value under testing conditions.

(2) All four composites exhibit low wear rate which, in the order of 10^{-5} mm^3/Nm (2.5–28.1 × 10^{-5} mm^3/Nm), especially for the composites of 8Mo and 12Mo, the values are below 8.8 × 10^{-5} mm^3/Nm.

(3) The 12Mo composite exhibits the lowest COF, while 8Mo has the highest COF and 0Mo/5Mo composites exhibited similar COFs under the given test conditions. From 25 to 600 °C, 8Mo and 12Mo composites exhibit a relatively low wear rate, while at 800 °C, 0Mo composite shows the best wear resistance properties.

(4) From 25 to 400 °C, the presence of Ag results in excellent lubricating performance, while at 600 and 800 °C, the effective lubricant is attributed to the formation of an oxidative glazed layer. The main wear mechanisms are abrasive and fatigue

wear at low-to-moderate temperatures, and it changes into abrasive wear at high temperatures.

(5) In further studies, we plan to investigate the influence of extreme testing conditions on the friction and wear behavior of nickel alloy matrix composites, such as ultralow temperature (−50 °C, −100 °C and −150 °C) and ultrahigh temperature (900 °C, 1000 °C and 1100 °C). The results obtained in this work will provide theoretical guidance for the design and preparation of high temperature solid lubricant materials.

Author Contributions: Methodology, J.Z.; investigation and writing—original draft preparation, Y.H.; data curation, L.Y.; Software, Z.J.; Softweare and resources, R.Z. All authors have read and agreed to the published version of the manuscript.

Funding: This work was supported by the National Natural Science Foundation of China (52105190 and 51905247), the Guangyue Young Scholar Innovation Team of Liaocheng University (LCUGYTD2023-02), and the Shandong Province Science and Technology Small and Medium Enterprises Innovation Ability Improvement Project (2022TSGC1220, 2022TSGC2575).

Data Availability Statement: Data are contained within the article.

Conflicts of Interest: The authors declare no conflicts of interest.

References

1. Voevodin, A.; Muratore, C.; Aouadi, S. Hard coatings with high temperature adaptive lubrication and contact thermal management: Review. *Surf. Coat. Technol.* **2014**, *257*, 247–265. [CrossRef]
2. Muratore, C.; Hu, J.; Voevodin, A. Adaptive nanocomposite coatings with a titanium nitride diffusion barrier mask for high-temperature tribological applications. *Thin Solid Films* **2007**, *515*, 3638–3643. [CrossRef]
3. Muratore, C.; Voevodin, A.; Hu, J.; Zabinski, J. Tribology of adaptive nanocomposite yttria-stabilized zirconia coatings containing silver and molybdenum from 25 to 700 °C. *Wear* **2006**, *261*, 797–805. [CrossRef]
4. Sarkar, M.; Mandal, N. Solid lubricant materials for high temperature application: A review. *Mater. Today Proc.* **2022**, *66*, 3762–3768. [CrossRef]
5. Rodriguez, A.; Jaman, M.; Acikgoz, O.; Wang, B.; Yu, J.; Grützmacher, P.; Rosenkranz, A.; Baykara, M. The potential of $Ti_3C_2T_X$ nano-sheets (MXenes) for nanoscale solid lubrication revealed by friction force microscopy. *Appl. Surf. Sci.* **2021**, *535*, 147664. [CrossRef]
6. Liang, J.; Yin, X.; Lin, Z.; Chen, S.; Liu, C.; Wang, C. Microstructure and wear behaviors of laser cladding in-situ synthetic (TiB_x+TiC)/(Ti_2Ni+TiNi) gradient composite coatings. *Vacuum* **2020**, *176*, 109305. [CrossRef]
7. Zhou, Z.; Liu, X.; Zhuang, S.; Yang, X.; Wang, M.; Sun, C. Preparation and high temperature tribological properties of laser in-situ synthesized self-lubricating composite coatings containing metal sulfides on Ti6Al4V alloy. *Appl. Surf. Sci.* **2019**, *481*, 209–218. [CrossRef]
8. Zhu, S.; Yu, Y.; Cheng, J.; Qiao, Z.; Yang, J.; Liu, W. Solid/liquid lubrication behavior of nickel aluminum-silver alloy under seawater condition. *Wear* **2019**, *420*, 9–16. [CrossRef]
9. Muratore, C.; Voevodin, A. Chameleon coatings: Adaptive surfaces to reduce friction and wear in extreme environments. *Annu. Rev. Mater. Res.* **2009**, *39*, 297–324. [CrossRef]
10. Zhen, J.; Zhen, C.; Han, Y.; Yuan, L.; Yang, L.; Yang, T.; Guo, S. High-temperature friction and wear behavior of nickel-alloy matrix composites with the addition of molybdate. *Lubricants* **2023**, *11*, 516. [CrossRef]
11. Ouyang, J.; Li, Y.; Zhang, Y.; Wang, Y.; Wang, Y. High-temperature solid lubricants and self-lubricating composites: A critical review. *Lubricants* **2022**, *10*, 177. [CrossRef]
12. Kumar, R.; Antonov, M.; Varga, M.; Hussainova, I.; Rodriguez Ripoll, M. Synergistic effect of Ag and MoS_2 on high-temperature tribology of self-lubricating NiCrBSi composite coatings by laser metal deposition. *Wear* **2023**, *532*, 205114. [CrossRef]
13. Moskalewicz, T.; Wendler, B.; Czyrska-Filemonowicz, A. Microstructure of nanocomposite carbon-, MoS_2- and MoO_3-based solid-lubricant coatings. *IOP Conf. Ser. Mater. Sci. Eng.* **2014**, *55*, 012012. [CrossRef]
14. Liu, C.; Chen, L.; Zhou, J.; Zhou, H.; Chen, J. Tribological properties of adaptive phosphate composite coatings with addition of silver and molybdenum disulfide. *Appl. Surf. Sci.* **2014**, *300*, 111–116. [CrossRef]
15. Yang, J.; Jiang, Y.; Hardell, J.; Prakash, B.; Fang, Q. Influence of service temperature on tribological characteristics of self-lubricant coatings: A review. *Front. Mater. Sci.* **2013**, *7*, 28–39. [CrossRef]
16. Sliney, H. Wide temperature spectrum self-lubricating coatings prepared by plasma spraying. *Thin Solid Films* **1979**, *64*, 211–217. [CrossRef]
17. Dellacorte, C.; Edmond, B. *Preliminary Evaluation of PS300: A New Self-Lubricating High Temperature Composite Coating for Use to 800 °C*; NASA TM 107056; NASA: Washington, DC, USA, 1 November 1995.
18. Dellacorte, C. A New Foil Air Bearing Test Rig for Use to 700 °C and 70,000 rpm. *Tribol. Trans.* **1998**, *41*, 335–340. [CrossRef]

19. Stanford, M.; Yanke, A.; DellaCorte, C. *Thermal Effects on a Low Cr Modification of PS304 Solid Lubricant Coating*; NASA/TM-2004-213111; NASA: Washington, DC, USA, 1 June 2004.
20. DellaCorte, C.; Stanford, M.; Thomas, F.; Edmonds, B. *The Effect of Composition on the Surface Finish of PS400: A New High Temperature Solid Lubricant Coating*; NASA/TM-2010-216774; NASA: Washington, DC, USA, 1 September 2010.
21. Dellacorte, C.; Lukaszewicz, V.; Valco, M.; Radil, K.; Heshmat, H. Performance and durability of high temperature foil air bearings for oil-free turbomachinery. *Tribol. Trans.* **2000**, *43*, 774–780. [CrossRef]
22. Voevodin, A.; O'neill, P.; Zabinski, J. WC/DLC/WS_2 nanocomposite coatings for aerospace tribology. *Tribol. Lett.* **1999**, *6*, 75–78. [CrossRef]
23. Baker, C.; Hu, J.; Voevodin, A. Preparation of Al_2O_3/DLC/Au/MoS_2 chameleon coatings for space and ambient environments. *Surf. Coat. Technol.* **2006**, *201*, 4224–4229. [CrossRef]
24. Gao, H.; Otero-de-la-Roza, A.; Gu, J.; Stone, D.; Aouadi, S.; Johnson, E.; Martini, A. (Ag, Cu)-Ta-O ternaries as high-temperature solid-lubricant coatings. *ACS Appl. Mater. Interfaces* **2015**, *7*, 15422–15429. [CrossRef] [PubMed]
25. Stone, D.; Liu, J.; Singh, D.; Muratore, C.; Voevodin, A.; Mishra, S.; Rebholz, C.; Ge, Q.; Aouadi, S. Layered atomic structures of double oxides for low shear strength at high temperatures. *Scr. Mater.* **2010**, *62*, 735–738. [CrossRef]
26. Aouadi, S.; Singh, D.; Stone, D.; Polychronopoulou, K.; Nahif, F.; Rebholz, C.; Muratore, C.; Voevodin, A. Adaptive VN/Ag nanocomposite coatings with lubricious behavior from 25 to 1000 °C. *Acta Mater.* **2010**, *58*, 5326–5331. [CrossRef]
27. Voevodin, A.; Capano, M.; Laube, S.; Donley, M.; Zabinski, J. Design of a Ti/TiC/DLC functionally gradient coating based on studies of structural transitions in Ti-C thin films. *Thin Solid Films* **1997**, *298*, 107–115. [CrossRef]
28. Corte, C.; Sliney, H. Composition optimization of self-lubricating chromium-carbide-based composite coatings for use to 760 °C. *Tribol. Trans.* **1987**, *30*, 77–83. [CrossRef]
29. Zhu, Z.; Chen, W.; Bian, Z.; Sun, Q.; Zheng, M.; Zhu, S.; Cheng, J.; Yang, J. Self-lubrication of high-entropy carbide matrix composites over a wide temperature range: The synergistic effect of silver and molybdenum component. *Wear* **2024**, *546*, 205341. [CrossRef]
30. Zhang, Z.; Gao, Y.; Cheng, J.; Gan, X.; Liu, C.; Zhou, K. Development of Cu-15Ni-8Sn/MoS_2 self-lubricating composites with desirable mechanical and friction properties. *Wear* **2024**, *550*, 205428. [CrossRef]
31. Qu, C.; He, B.; Cheng, X.; Wang, H. Microstructure and wear characteristics of laser-clad Ni-based self-lubricating coating incorporating MoS_2/Ag for use in high temperature. *J. Mater. Res. Technol.* **2024**, *33*, 4481–4492. [CrossRef]
32. Cao, W.; Yan, W.; Yang, X.; Li, Z.; Geng, J.; Dong, Y.; Zhang, Y.; Qi, X. Multiscale study on the solid-liquid synergistic lubrication mechanism of graphite and liquid lubricant in polymer composites. *Carbon* **2024**, *230*, 119605. [CrossRef]
33. Bian, Z.; Zheng, M.; Sun, Q.; Zhu, Z.; Zhu, S.; Cheng, J.; Liu, X.; Tan, H.; Yang, J. High-temperature tribological properties of NiCr-Cr_3C_2 cermet coatings in fluoride molten salts. *Tribol. Int.* **2024**, *200*, 110150. [CrossRef]
34. Ye, F.; Lou, Z.; Wang, Y.; Liu, W. Wear mechanism of Ag as solid lubricant for wide range temperature application in micro-beam plasma cladded Ni60 coatings. *Tribol. Int.* **2022**, *167*, 107402. [CrossRef]
35. Zeng, Q. Influence of $CePO_4$ on high temperature anti-friction and anti-wear behaviors of nickel-based h-BN composite coatings. *Diam. Relat. Mater.* **2024**, *148*, 111421. [CrossRef]
36. Zheng, C.; Huang, K.; Mi, T.; Li, M.; Yi, X. Laser cladding Ni60 @ WC/Cu encapsulated rough MoS2 self-lubricating wear resistant composite coating and ultrasound-assisted optimization. *Ceram. Int.* **2024**, *50*, 36555–36569. [CrossRef]
37. Qin, Q.; Wang, T. Effect of mo content on the microstructure and properties of powder metallurgy iron based friction materials. *J. Phys. Conf. Ser.* **2024**, *2670*, 012071. [CrossRef]
38. Behera, N.; Ramesh, M.R.; Rahman, M.R. Elevated temperature wear and friction performance of WC-CoCr/Mo and WC-Co/NiCr/Mo coated Ti-6Al-4V alloy. *Mater. Charact.* **2024**, *215*, 114207. [CrossRef]
39. Zhen, Y.; Chen, M.; Yu, C.; Yang, Z.; Qi, Y.; Wang, F. High temperature self-lubricating Ti-Mo-Ag composites with exceptional high mechanical strength and wear resistance. *J. Mater. Sci. Technol.* **2024**, *180*, 80–90. [CrossRef]
40. Moussaoui, A.; Abboudi, A.; Aissani, L.; Belgroune, A.; Cheriet, A.; Alhussein, A.; Rtimi, S. Effect of Mo addition on the mechanical and tribological properties of magnetron sputtered TiN films. *Surf. Coat. Technol.* **2023**, *470*, 129862. [CrossRef]
41. Cui, G.; Han, W.; Zhang, W.; Li, J.; Kou, Z. Friction and wear performance of laser clad Mo modified Stellite 12 matrix coatings at elevated temperature. *Tribol. Int.* **2024**, *196*, 109738. [CrossRef]
42. Zhen, J.; Han, Y.; Chen, J.; Cheng, J.; Zhu, S.; Yang, J.; Kong, L. Influence of Mo and Al elements on the vacuum high temperature tribological behavior of high strength nickel alloy matrix composites. *Tribol. Int.* **2019**, *131*, 702–709. [CrossRef]

Disclaimer/Publisher's Note: The statements, opinions and data contained in all publications are solely those of the individual author(s) and contributor(s) and not of MDPI and/or the editor(s). MDPI and/or the editor(s) disclaim responsibility for any injury to people or property resulting from any ideas, methods, instructions or products referred to in the content.